PHYSICAL REVIEW B **84**, 035431 (2011)

Spin-polarized and valley helical edge modes in graphene nanoribbons

Zhenhua Qiao,[1] Shengyuan A. Yang,[1] Bin Wang,[2] Yugui Yao,[1,3] and Qian Niu[1,4,*]

[1]*Department of Physics, The University of Texas at Austin, Austin, Texas 78712, USA*
[2]*Department of Physics, The University of Hong Kong, Hong Kong, China*
[3]*Institute of Physics, Chinese Academy of Sciences, Beijing 100190, China*
[4]*International Center for Quantum Materials, Peking University, Beijing 100871, China*

(Received 26 May 2011; published 25 July 2011)

We investigate the electronic properties of zigzag-terminated graphene nanoribbons in the presence of a staggered sublattice potential. We show that due to the edge ferromagnetism, spin-polarized dispersive edge modes with well-defined valley indices can appear inside the bulk band gap opened by the inversion symmetry breaking. These edge modes are helical with respect to their valley indices, hence are robust against scattering from smooth disorder potentials. We further propose a concrete system with a zigzag graphene nanoribbon grown on top of a hexagonal boron-nitride substrate to realize such edge modes. These edge states could be utilized as perfect spin filters or analyzers in spintronics applications.

DOI: 10.1103/PhysRevB.84.035431　　　PACS number(s): 73.20.−r, 73.22.Pr, 75.75.−c

I. INTRODUCTION

The existence of a set of edge states is an important and interesting property of the zigzag-terminated graphene nanoribbons.[1] Without electron-electron interaction, the edge states form a completely flat edge band connecting the two valleys K and K' with a large momentum separation,[1,2] and their presence is dictated by the bulk topological charge.[3] With flat dispersion, the edge band cannot be used as conducting channels. When the electron-electron interaction is taken into account, due to the singular density of states of the flat band, spins on the edge become spontaneously polarized, resulting in the edge ferromagnetism.[4–6] The spin-polarized edge states then become dispersive, allowing them to carry currents. However, without a bulk band gap, the edge states are still of little use because their effects would be overwhelmed by the contribution from the bulk states.

Motivated by the many interests of utilizing these unusual edge states for various applications[4,7] and particularly the recent advance in fabricating graphene nanoribbons with precise edge termination,[8–10] we propose to realize in the zigzag-edged graphene nanoribbons the spin-polarized valley helical edge states inside a bulk band gap opened by a staggered sublattice potential. The sublattice potential can be realized by coupling to a substrate such as the hexagonal boron-nitride[11] or the silicon carbide.[12] Our proposition makes the edge states useful as perfect spin/valley conducting channels. For proper values of the spin splitting and the band gap, the edge states contributing to transport can acquire well-defined valley indices hence they remain robust against the scattering from smooth disorder potentials due to the valley protection. Based on first-principles calculations, we point out a concrete way to realize such edge states by growing a zigzag terminated graphene nanoribbon on top of a hexagonal boron-nitride substrate. The phenomena we predict here will not only be of academic interest but will also be important for spintronics and valleytronics applications.

II. TIGHT-BINDING MODEL

Figure 1 illustrates the schematic setup of a zigzag-edged graphene nanoribbon in the presence of a staggered AB-sublattice potential. The tight-binding Hamiltonian that incorporates phenomenologically the edge spin polarization can be written as

$$H = -t\sum_{\langle ij\rangle\alpha} c_{i\alpha}^{\dagger}c_{j\alpha} + M\sum_{i=1,N;\alpha,\beta} c_{i\alpha}^{\dagger}\sigma_{\alpha\beta}^{z}c_{i\beta} + \sum_{i,\alpha} U_i c_{i\alpha}^{\dagger}c_{i\alpha}, \quad (1)$$

where $c_{i\alpha}^{\dagger}(c_{i\alpha})$ is the electron creation (annihilation) operator on site i with spin α, and σ_z is the z component of the real spin Pauli matrices. α and β denote the real spin indices. The first term describes the nearest-neighbor hopping with t being the amplitude of the hopping energy. The second term represents the effect of edge ferromagnetism involving only the outmost boundary atoms ($i = 1,N$). This term stems microscopically from the electron-electron interaction, but at this stage we capture this effect phenomenologically with a mean-field parameter M whose value will be determined later from the first-principles calculations. The last term corresponds to the staggered AB-sublattice potential. We set $U_i = \Delta/2$ for sublattice A (○), and $U_i = -\Delta/2$ for sublattice B (●). In the following analysis, we measure the energy ε, the magnetization M, the potential Δ, and the disorder strength W in units of the hopping energy t.

We first make a Fourier transform on the Hamiltonian in Eq. (1) along the edge direction which we take as the y axis such that each eigenstate is labeled with a good quantum number k_y. The energy spectrum is obtained by a subsequent numerical diagonalization and the results are plotted versus k_y in Fig. 2 for different values of the parameter M. Here the ribbon width is fixed to $N = 800$ (about 852 Å). When considering the edge magnetism at both boundaries, there are two possible configurations: ferromagnetic ($M|_{i=1} = M|_{i=N}$) and antiferromagnetic ($M|_{i=1} = -M|_{i=N}$). It is known that for small size systems (i.e., $N < 32$), the antiferromagnetic configuration is the lowest-energy ground state.[4] When the size becomes larger, both configurations can serve as the ground state. In the following, we only show the band structures of the ferromagnetic case. For clarity, we use different lines to distinguish the edge bands located at the different boundaries, i.e., the solid (dashed) lines represent the states located at the left (right) boundary.

©2011 American Physical Society

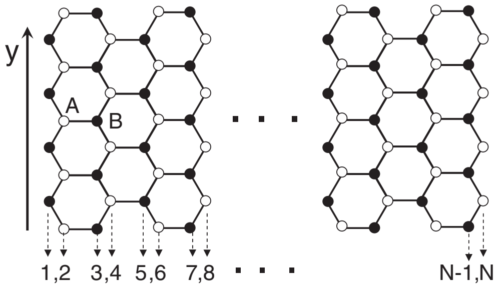

FIG. 1. Schematic figure of a zigzag-edged graphene nanoribbon along y axis. A (○) and B (●) sublattices are subjected to staggered potentials: $U_A = +\Delta/2$ and $U_B = -\Delta/2$. The edge magnetization M is considered only at the outmost boundary atoms labeled as 1 and N.

In Fig. 2(a), a staggered sublattice potential with $\Delta = 0.4$ is considered but M is set to be zero, i.e., no edge ferromagnetism. One can observe that a bulk energy gap $\Delta = 0.4$ is opened due to the inversion symmetry breaking induced by the staggered sublattice potential, and there are doubly degenerate flat bands connecting the two Dirac points K and K' at the band edges $\varepsilon = \pm\Delta/2$. A bulk band gap indicates an insulating state, and the gap size is only determined by the amplitude of the staggered sublattice potentials. In Figs. 2(b)– 2(d), besides the fixed sublattice potentials $\Delta = 0.4$, the edge magnetization is switched on by taking M to be 0.6 (b), 1.0 (c), and 1.4 (d), respectively. We find that, due to the different degrees of localization of the states in the edge bands,[3] the magnitude of the energy splitting of the edge bands is k_y dependent: the spin-up edge band bends upward, while the spin-down edge band bends downward. This makes the edge band dispersive hence capable of conducting charge currents. Moreover, along with the increase of the edge magnetization M from 0.6 [see Fig. 2(b)] to 1.0 [see Fig. 2(c)], the spin-down edge band which is initially located at the conduction-band edge gradually approaches the bulk valence band, and eventually touches and merges into the bulk valence band (at $M_0 \simeq 1.4$). Similarly, the spin-up edge band from the valence flat bands bends upward, and eventually touches the bulk conduction bands. This creates gapless edge modes tied to each valley, which is similar to the findings in Ref. 3 except that the edge modes here are spin polarized.

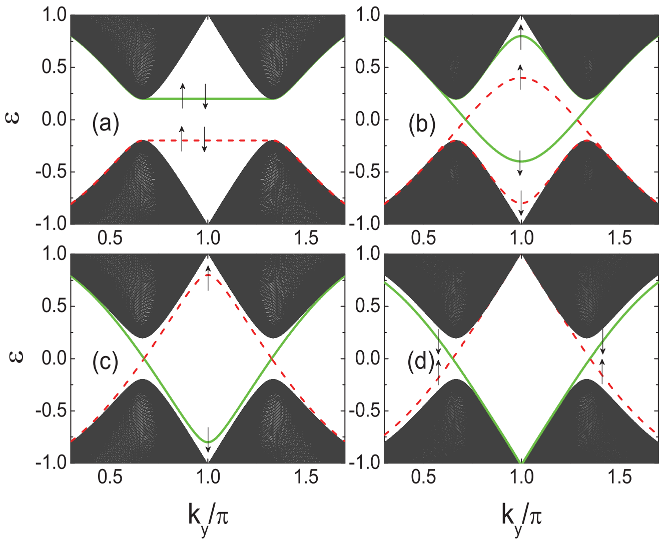

FIG. 2. (Color online) Evolution of the band structure of the zigzag-edged graphene nanoribbon with a fixed width $N = 800$. (a) When the staggered sublattice potential $\Delta = 0.4$ is applied, an bulk gap is opened, and the flat-bands are doubly-degenerate; (b)–(d) The edge magnetism is further switched on with $M = 0.6, 1.0$, and 1.4, respectively. The flat bands become spin split: spin-up edge band bends upward, while spin-down edge band bends downward. The green solid (red dashed) curves represent the edge states from the left (right) boundary.

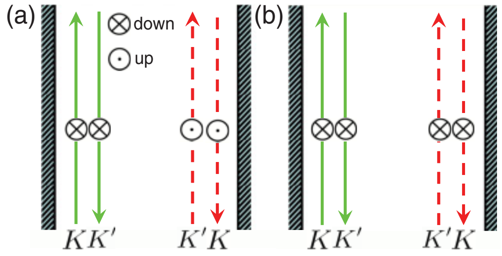

FIG. 3. (Color online) Schematic plot of the edge states propagation directions. (a) When the spin polarizations on the two boundaries are parallel, spin-up (spin-down) polarized valley helical edge states propagate along the right (left) boundary; (b) when the spin polarizations on the two boundaries are antiparallel, the edge states at each boundary have the same spin polarization.

From the energy dispersion together with the location of the edge states in Figs. 2(b)–2(d), one can easily obtain the edge states' propagation directions as shown in Fig. 3(a). One can observe that the edge states at opposite boundaries have opposite spin polarizations, and their propogation directions are tied to their valley indices. In addition, we also plot the edge states' propagation for the antiferromagnetic configuration in Fig. 3(b). The only difference compared to Fig. 3(a) is that the edge states located at both boundaries have the same spin polarization. For both cases the system state can be termed as the spin-polarized quantum valley Hall state. For the normal quantum valley Hall state proposed before,[13] there is actually no gapless edge state. In contrast, the spin-polarized quantum valley Hall state we find here is characterized by spin-polarized gapless edge states. The situation is similar to that for the gated bilayer graphene case.[14]

III. ROBUSTNESS OF SPIN-POLARIZED EDGE MODES

From the above analysis, we notice that for a fixed bulk gap size, the spin-polarized edge state is gapped for a weak edge magnetization M, and the edge states become gapless when M approaches a critical value M_c. These edge states provide conducting channels for the spin-polarized transport when the Fermi level goes across them in the gap. However, to be useful for practical applications, they need to be robust against impurity scattering. In the following, we will investigate the robustness of the edge state in the presence of impurities, and show that the spin-polarized edge states are robust against impurity scattering due to the large momentum separation between the valleys K and K'.

It is known that the impurity scattering in graphene mainly comes from the long-range Coulomb scatterers.[15] We assume that the impurity potential V_i at each site i takes a Gaussian form:[16]

$$V_i = \sum_j w_j \times \exp\left(-\frac{|\mathbf{r}_j - \mathbf{r}_i|^2}{2 \times \xi^2}\right), \tag{2}$$

where the summation is over all sites, w_j is the local disorder strength at site j and is uniformly distributed in the interval $[-w/2, w/2]$. ξ is the correlation length in units of the nearest-neighbor distance. In our calculation, the disorder term is incorporated into Eq. (1) as $\sum_{i,\alpha} V_i c^{\dagger}_{i\alpha} \sigma c_{i\alpha}$, where $\sigma = \sigma_0$, $\sigma_{x/y}$, σ_z correspond to scalar, spin-flip, and Zeeman-type disorders.[17] For the convenience of comparison, we define an effective on-site disorder strength W in terms of ξ and w:[18]

$$W = w \times (4\xi^2 + 1). \tag{3}$$

The numerical simulations are performed within the same setup of Ref. 19 by including only the left and right semi-infinite leads, i.e., a two-terminal configuration for conductance calculation. The two-terminal conductance is calculated from the Landauer-Büttiker formula:[20]

$$G = \frac{e^2}{h} \mathrm{Tr}[\Gamma_R G^r \Gamma_L G^a], \tag{4}$$

where $G^{r,a}$ are the retarded and advanced Green's functions of the central disordered region. The quantities $\Gamma_{L/R}$ are the linewidth functions describing the coupling between the left/right lead and the scattering region, and can be obtained from $\Gamma_p = i(\Sigma^r_p - \Sigma^a_p)$. Here, $\Sigma^{r/a}_p$ is the retarded/advanced self-energy of the pth semi-infinite lead ($p = L, R$), and can be numerically evaluated using the recursive transfer-matrix method.[21]

In Fig. 3(a), we can see that for the edge state associated with valley K and located at the left boundary, it has two possible backscattering paths: (1) scattered into states associated with valley K' located at the left boundary; (2) scattered into states associated with the same valley K located at the right boundary. The process via the second path is suppressed because the spatial separation protects the edge state from scattering to the opposite boundary far away, which is similar to the situation in the quantum Hall effect.[22] Therefore the state can only be scattered via the first path into the states with opposite valley index. Because the states propagating along opposite directions at the same boundary possess the same spin, the scalar-type and Zeeman-type disorders should have similar effects, which has been confirmed by our numerical calculations. On the other hand, the spin-flip disorders cannot couple the states with the same spin. Therefore in the following, we will only show the result for the short-range and the long-range nonmagnetic (scalar) disorders.

Figure 4 plots the sample averaged two-terminal conductance $\langle G \rangle$ as a function of the effective disorder strength W for three different Fermi energies $\varepsilon = -0.1$, 0, 0.1, respectively. For clarity, we only consider the ferromagnetism at one boundary. The edge magnetization is set to be $M = 0.6$. Each data point represents the average over 20 000 sample configurations. Fig. 4(a) is for the long-range disorder case with the correlation length $\xi = 4$. We observe that for all three energies inside the bulk band gap, the average conductances $\langle G \rangle$ are robust against weak disorders, e.g., for $W < 2.0$ the conductance is exactly quantized to be 1 in units of e^2/h without any fluctuation. When $W > 2.0$, we find that $\langle G \rangle$ at $\varepsilon = -0.1$ decreases, and that at $\varepsilon = 0.1$ is the most robust one. This can be explained from the band structure as shown in Fig. 2(b). One can see that the two edge states for a fixed Fermi energy have a large momentum separation when the Fermi energy is near the upper band bottom (e.g., at $\varepsilon = 0.1$). The separation decreases when the Fermi energy is approaching the valence band top. The large momentum separation (on the scale of valley separation) suppresses the long-range impurity scattering hence the states at $\varepsilon = -0.1$ are more robust.

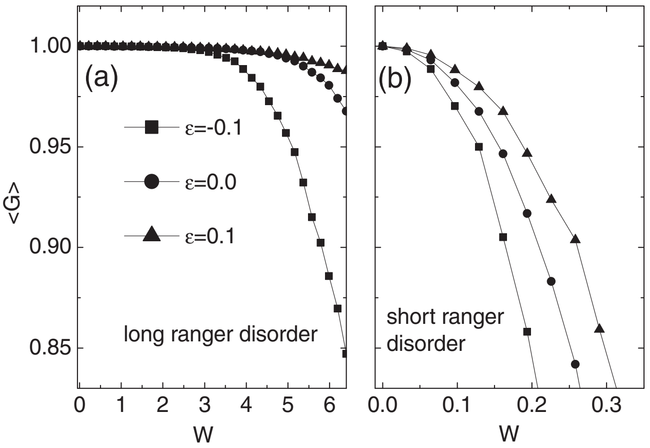

FIG. 4. Average conductance $\langle G \rangle$ in units of e^2/h versus the effective disorder strength W for scalar-type disorders at $\Delta = 0.4$ and $M = 0.6$ for different Fermi energies $\varepsilon = -0.1$ (square), 0 (circle), 0.1 (triangle), respectively. (a) For long-range disorder ($\xi = 4$), the edge states can be exactly quantized for disorder strength up to $W = 0.8$; (b) for short-range disorder ($\xi = 0$), the conductance quickly decreases as W increases above 0.1. 20 000 ensembles are collected for each data point in the figure. Note that in this calculation we only consider the ferromagnetism at one boundary to emphasize the disorder effect of only one conducting channel.

Figure 4(b) shows the average conductance as a function of the short-range ($\xi = 0$) nonmagnetic disorders, with other parameters being the same as that in Fig. 4(a). We find that the edge states are very sensitive to the short-range disorders and are easily destroyed. This is because the short-range disorders can easily mix the separated valleys thus scatter back the edge states. Therefore we conclude that our valley associated spin-polarized edge modes are robust against smooth disorder scattering, which is known to be dominating in graphene.

IV. FIRST-PRINCIPLES CALCULATIONS

So far, we have investigated the properties of the edge modes in a zigzag-edged graphene nanoribbon by using a phenomenological tight-binding model. In the following, from first-principles calculations, we confirm the validity of the phenomenological approach above and also provide a concrete system that is of a zigzag-edged graphene nanoribbon grown on top of a hexagonal boron-nitride substrate.

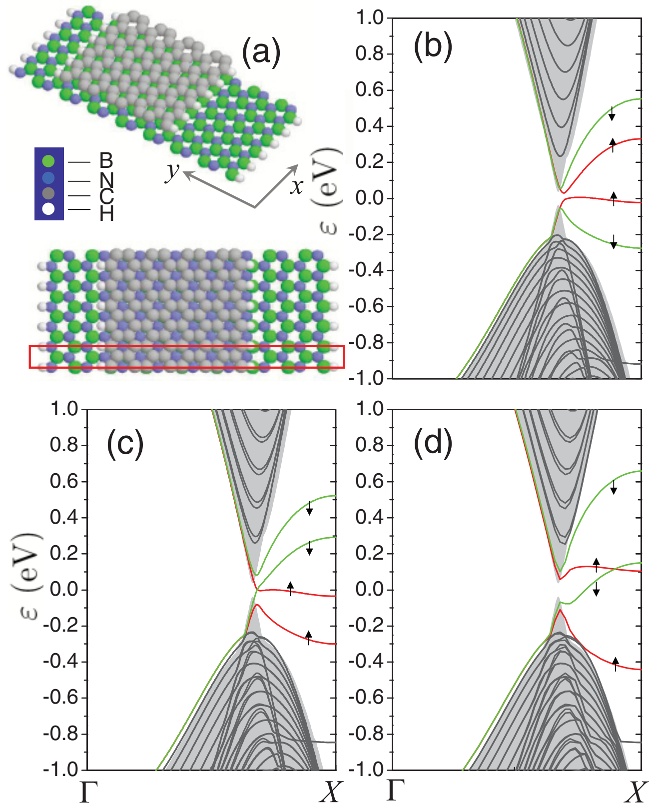

FIG. 5. (Color online) (a) Atomic structure of the hydrogen-terminated zigzag-edged graphene nanoribbons on top of a single layer of hexagonal boron-nitride. The red square shows a supercell. Upper: side view; lower: top view. (b) Band structure of spin antiparallel configurations (between two boundaries). In the bulk energy gap (the narrow energy window of the projected bulk band structure shown in light gray, Δ around 78 meV), only the spin-up states exist. A very small gap appears because of the weak interaction between the edges states on opposite boundaries, which is a finite-size effect. (c) Band structure for spin parallel case. Spin-up and spin-down states coexist in the gap. (d) When a voltage bias of 0.27 V is applied transversely, the upper (lower) edge states are shifted upward (downward), leaving only the spin-down states in the gap. Bands in red and green color represent the spin-up and the spin-down edge bands, respectively.

In the calculations, we take the lattice constant to be $a = 2.45$ Å, and inter-layer distance $d = 3.22$ Å.[11] Figure 5(a) illustrates the schematic configuration of the system. Here, we use N_1 (N_2) to label the width of graphene (boron-nitride), and $N_1 < N_2$. The single layer graphene and boron-nitride are AB stacked with nitrogen atoms on top of the hollow position. All the outmost boundary atoms are saturated with hydrogen atoms. The experimental values of the bond lengths 1.17 Å (B-H), 1.01 Å (N-H), and 1.09 Å (C-H) are used. The self-consistent ground-state calculations were performed within the nonequilibrium Green's function coupled with the density-functional theory scheme,[23] and the local-density approximation with exchange-correlation potential (LDA-PZ81) was used.[24]

Figures 5(b)–5(d) show the energy-band structures of the system with $N_1 = 96$ and $N_2 = 112$. In Fig. 5(b), the spin polarization at the two zigzag boundaries are arranged to be antiparallel. The gray region represents the continuum of bulk states (i.e., corresponding to a system with width approaching infinity). Our calculations show that a bulk band gap around 78 meV is opened. This is slightly larger than the value 53 meV calculated for the system of a single layer graphene placed on top of several layers of boron-nitride.[11] We find that only the spin-up polarized edge states lie inside the bulk gap, which is consistent with the tight-binding model discussion. Note that a small splitting δ appears inside the bulk gap. This arises from the weak interaction between the edges states on opposite boundaries, and will vanish with the increasing system width. Through external control methods (e.g., employing ferromagnetic insulators to control the spin polarization), one can manipulate the spin-polarization direction at individual boundaries, and achieve various device functions.

In Fig. 5(c), the spin polarization at the two zigzag boundaries are set to be parallel. We observe that the spin-up and spin-down states coexist in the bulk band gap, which is similar to the scenario in Fig. 2(b). Therefore by tuning a gate voltage, we can control the spin and valley indices of the electrons that pass through the structure. Another way to realize the spin and valley filtering function is to apply an external transverse bias.[4] Figure 5(d) is obtained from Fig. 5(c) by applying a transverse bias 0.27 V across the ribbon's width. One can see that the spin-up band is pushed upward outside the bulk gap, and only the spin-down band is left inside the gap. One can further notice that the applied bias only affects the edge states but not the bulk energy spectrum. Since only the spin-down edge band lies inside the bulk gap, it is more convenient to be used as a spin filter or a valley filter. These interesting properties of the spin-polarized valley helical edge states

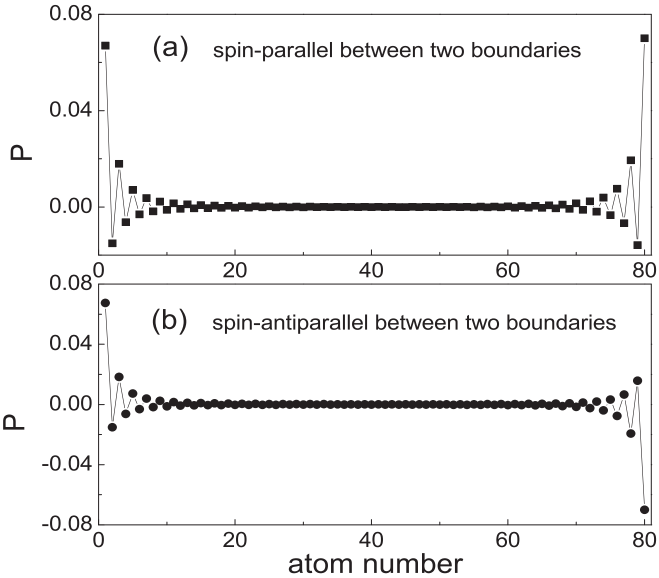

FIG. 6. Spin polarization for the carbon atoms inside a supercell. (a) For the spin-parallel configuration, the spin polarization is symmetric about the ribbon center; (b) for the spin antiparallel configuration, the spin polarization is antisymmetric about the ribbon center. Note that the amplitude of the spin polarization is exponentially decreased accompanying with oscillations between sublattice sites.

show great potential for the graphene-based spintronics[25] and valleytronics[26] devices. Similar spin-polarized edge modes also appear in the zigzag-edged boron-nitride nanoribbons with boron atoms at the boundaries.[27]

Finally we want to extract from the first-principles calculations the values of the relevant parameters in the corresponding tight-binding model. From Figs. 5(b) and 5(c), the strength of the edge magnetization should be $M = 0.287$ eV by taking the spin splitting at X point. From the bulk gap, we can get the substrate induced staggered AB sublattice potentials to be $U = \pm 39$ meV. In units of the hopping energy t, we have $M = 0.11t$ and $U = 0.02t$. The edge magnetization is intrinsic and independent of the external substrate, while the staggered potentials depend on the substrate. In Fig. 6, we exhibit the spin polarization of the carbon atoms inside a supercell for (a) spin-parallel and (b) spin-antiparallel configurations. Here the spin polarization is defined as $P = (n_\uparrow - n_\downarrow)/(n_\uparrow + n_\downarrow)$, where $n_{\uparrow/\downarrow}$ represents the number of charge carriers with spin up/down. We find that the amplitude of the spin polarization at one boundary is exponentially decreased from the outmost atom toward the center, accompanied with oscillations between A and B sublattices. In Fig. 6(a) the spin polarization is symmetric about the center, while in Fig. 6(b) it is antisymmetric about the center. In particular, the amplitude of spin polarization at the outmost atoms is much larger than the spin polarization at other atomic sites. This confirms that our phenomenological tight-binding model captures the main features of the physical system.

V. CONCLUSION

We have investigated the edge modes of zigzag-edged graphene nanoribbons in the presence of a staggered sublattice potential. We find that the edge states form spin-polarized valley helical conducting channels which are robust against smooth impurity potentials. Using first-principles calculation methods, we provide a specific system which exhibits such interesting edge modes. The system consists of a zigzag-edged graphene nanoribbon grown on top of a hexagonal boron-nitride substrate. The realization of such spin-polarized valley helical edge modes will facilitate the application of the graphene based spintronics and valleytronics devices.

ACKNOWLEDGMENTS

Z.Q. was supported by NSF (Grant No. DMR0906025) and Welch Foundation (Grant No. F-1255). Q.N. was supported by DOE (Grant No. DE-FG03-02ER45958, Division of Materials Science and Engineering) and Texas Advanced Research Program. Y.Y. was supported by NSF of China (Grant No. 10974231) and the MOST Project of China (Grants No. 2007CB925000 and No. 2011CBA00100).

---

[*] On leave from the University of Texas at Austin.

[1] C. W. J. Beenakker, Rev. Mod. Phys. **80**, 1337 (2008); A. H. Castro Neto, F. Guinea, N. M. R. Peres, K. S. Novoselov, and A. K. Geim, *ibid.* **81**, 109 (2009).

[2] K. S. Novoselov, A. K. Geim, S. V. Morozov, D. Jiang, Y. Zhang, S. V. Dubonos, I. V. Grigorieva, and A. A. Firsov, Science **306**, 666 (2004); Y. B. Zhang, Y.-W. Tan, H. L. Stormer, and Philip Kim, Nature (London) **438**, 201 (2005).

[3] W. Yao, S. A. Yang, and Q. Niu, Phys. Rev. Lett. **102**, 096801 (2009).

[4] Y. W. Son, M. L. Cohen, and S. G. Louie, Nature (London) **444**, 347 (2006).

[5] J. Jung, T. Pereg-Barnea, and A. H. MacDonald, Phys. Rev. Lett. **102**, 227205 (2009); J. Jung and A. H. MacDonald, Phys. Rev. B **79**, 235433 (2009); J. Jung, *ibid.* **83**, 165415 (2011); J. Zhou, Q. Wang, Q. Sun, X. S. Chen, Y. Kawazoe, and P. Jena, Nano Lett. **9**, 3867 (2009); L. Yang, M. L. Cohen, and S. G. Louie, Phys. Rev. Lett. **101**, 186401 (2008).

[6] C. G. Tao, L. Y. Jiao, O. V. Yazyev, Y.-C. Chen, J. J. Feng, X. W. Zhang, R. B. Capaz, J. M. Tour, A. Zettl, S. G. Louie, H. J. Dai, and M. F. Crommie, Nat. Phys. doi:10.1038/nphys1991.

[7] K. A. Ritter and J. W. Lyding, Nat. Mater. **8**, 235 (2009).

[8] L. Jiao, L. Zhang, X. R. Wang, G. Diankov, and H. J. Dai, Nature (London) **458**, 877 (2009); D. V. Kosynkin, A. L. Higginbotham, A. Sinitskii, J. R. Lomeda, A. Dimiev, B. K. Price, and J. M. Tour, *ibid.* **458**, 872 (2009).

[9] L. C. Campos, V. R. Manfrinato, J. D. Sanchez-Yamagishi, J. Kong, and P. Jarillo-Herrero, Nano Lett. **9**, 2600 (2009).

[10] X. Jia, M. Hofmann, V. Meunier, B. G. Sumpter, J. Campos-Delgado, J. M. Romo-Herrera, H. Son, Y.-P. Hsieh, A. Reina, J. Kong, M. Terrones, and M. S. Dresselhaus, Science **323**, 1701 (2009); Ç. Ö. Girit, J. C. Meyer, R. Erni, M. D. Rossell, C. Kisielowski, L. Yang, C.-H. Park, M. F. Crommie, M. L. Cohen, S. G. Louie, and A. Zettl, *ibid.* **323**, 1705 (2009).

[11] G. Giovannetti, P. A. Khomyakov, G. Brocks, P. J. Kelly, and J. van den Brink, Phys. Rev. B **76**, 073103 (2007).

[12] S. Y. Zhou, G.-H. Gweon, A. V. Fedorov, P. N. First, W. A. De Heer, D.-H. Lee, F. Guinea, A. H. Castro Neto, and A. Lanzara, Nat. Mater. **6**, 770 (2009).

[13] D. Xiao, W. Yao, and Q. Niu, Phys. Rev. Lett. **99**, 236809 (2007).

[14] W.-K. Tse, Z. H. Qiao, Y. G. Yao, A. H. MacDonald, and Q. Niu, Phys. Rev. B **83**, 155447 (2011).

[15] F. Miao, S. Wijeratne, Y. Zhang, U. C. Coskun, W. Bao, and C. N. Lau, Science **317**, 1530 (2007); Y. Y. Zhang, J.-P. Hu, X. C. Xie, and W. M. Liu, Physica B **404**, 2259 (2007).

[16] K. Wakabayashi, Y. Takane, M. Yamamoto, and M. Sigrist, New J. Phys. **11**, 095016 (2009).

[17] S. A. Yang, H. Pan, Y. Yao, and Q. Niu, Phys. Rev. B **83**, 125122 (2011).

[18] The factor of 4 is a numerical fitting number for a finite-size scattering regime, which is slightly smaller than 2π for an infinite two-dimensional scattering regime. The factor 2π can be obtained by setting all the on-site disorders to unity.

[19] Z. H. Qiao, J. Wang, Y. D. Wei, and H. Guo, Phys. Rev. Lett. **101**, 016804 (2008).

[20] S. Datta, *Electronic Transport in Mesoscopic Systems* (Cambridge University Press, Cambridge, UK, 2003).

[21] M. P. López-Sancho, J. M. López-Sancho, and J. Rubio, J. Phys. F **14**, 1205 (1984); **15**, 851 (1985).

[22] M. Büttiker, Phys. Rev. B **38**, 9375 (1988).

[23] J. Taylor, H. Guo, and J. Wang, Phys. Rev. B **63**, 245407 (2001); **63**, 121104 (2001).

[24] J. P. Perdew and A. Zunger, Phys. Rev. B **23**, 5048 (1981).

[25] I. Zutic, J. Fabian, and S. Das Sarma, Rev. Mod. Phys. **76**, 323 (2004).

[26] A. Rycerz, J. Tworzyd, and C. W. J. Beenakker, Nat. Phys. **3**, 172 (2007); I. Martin, Ya. M. Blanter, and A. F. Morpurgo, Phys. Rev. Lett. **100**, 036804 (2008); J. Li, A. F. Morpurgo, M. Büttiker, and I. Martin, Phys. Rev. B **82**, 245404 (2010).

[27] F. Zheng, G. Zhou, Z. Liu, J. Wu, W. Duan, B.-L. Gu, and S. B. Zhang, Phys. Rev. B **78**, 205415 (2008).